Supramolecular Self-Assembly between cyclopentanocucurbit[6]uril and 1H-benzotriazole

Dai Xue,[a] Xin Xiao,[a]* Jun Zheng,[a] Yue Ma,[b] Na-Qin Yang,[a] Carl Redshaw,[c] Pei-Hua Ma,[a]*

[a] Key Laboratory of Macrocyclic and Supramolecular Chemistry of Guizhou Province, Institute of Applied Chemistry, Guizhou University, Guiyang 550025, China.

[b] Guiyang College of Humanities and Science, Guiyang 550025, China

[c] Chemistry, School of Natural Sciences, University of Hull, Hull HU6 7RX, U.K

E-mail: gyhxxiaoxin@163.com, xxiao@gzu.edu.cn (Xin. Xiao)

phma@gzu.edu.cn (Pei-Hua Ma)

Abstract: In this paper, the host-guest supramolecular interactions between cyclopentanocucurbit[6]uril with 1*H*-benzotriazole (BTA) have been investigated using NMR spectroscopy, isothermal titration calorimetry (ITC), MALDI-TOF mass spectrometry, IR spectroscopy, thermogravimetric analysis and single crystal X-ray diffraction. The results show that there is a 1:1 mode of inclusion in BTA@CyP$_6$Q[6], which forms a supramolecular framework through hydrogen bonds and dipole interactions. In addition, the benzene ring of the BTA molecule entered the cavity of CyP$_6$Q[6], while the triazole part was at the port of the CyP$_6$Q[6]. According to the ITC data, the complexation process for BTA with CyP$_6$Q[6] is mainly driven by enthalpy.

Keywords: CyP$_6$Q[6], BTA, Supramolecular framework, Crystal structure, enthalpy drive

Introduction

Supramolecular chemistry is the chemistry of molecular aggregates based on non-covalent interactions between molecules [1]. It involves many fields such as life science, medicine and physics [2-5], and is an interdisciplinary subject with a wide range of potential research applications. As one of the emerging branches of supramolecular chemistry, the chemistry of the cucurbit[*n*]uril [Q[*n*]] family plays a very important function in supramolecular chemistry [6]. The special rigid structure of the Q[*n*]s can not only interact with ions, but also can be assembled with organic molecules, so as to construct different supramolecular assemblies based on cucurbit[*n*]urils [7-10]. They have been widely used in different areas such as adsorption, electron transfer, recognition, separation, cell imaging, pharmaceutical carriers and catalysis [11-19]. As research progresses, problems associated with ordinary cucurbit[*n*]urils have been recognized, such as poor solubility, low activity of reaction sites, both of which have hampered modification and so on have greatly limited the development and application of cucurbit[*n*]uril chemistry [20-21]. In

view of the above problems, research has focused on developing new routes to modifying Q[*n*]s and improving their structural properties in terms of enhancing solubility and reactivity. More and more cucurbit[*n*]urils have now been synthesized, such as methyl-substituted cucurbit[*n*]urils, hydroxyl-substituted cucurbit[*n*]urils, phenyl-substituted cucurbit[*n*]urils, cyclobutyl-substituted cucurbit[*n*]urils, cyclohexyl-substituted cucurbit[*n*]urils, cyclopentyl-substituted cucurbit[*n*]urils, hemicucurbit[*n*]urils and inverted cucurbit[*n*]urils [22-29]. Among them, $CyP_6Q[6]$ not only has a highly symmetrical structure, but also improves the shortcoming of poor solubility of ordinary cucurbit[*n*]urils and greatly expands the application range for cucurbit[*n*]urils [30]. In recent years, some research has been conducted on the interaction of cyclopentyl-substituted cucurbit[*n*]urils with organic guests and metal ions [31-33], but such studies remain scant.

For this article, the supramolecular assembly of $CyP_6Q[6]$ and 1*H*-benzotriazole (BTA), prepared in the presence of the inducer $ZnCl_2$, namely ($BTA@Cy_{P6}Q[6]$) was confirmed as a supramolecular framework by single crystal X-ray diffraction analysis. The interaction modes of the host and guest were investigated by means of ^1H NMR spectroscopy, isothermal titration calorimetry (ITC), MALDI-TOF mass spectrometry, IR spectroscopy and thermogravimetric analysis. The starting materials employed herein are shown in Figure 1.

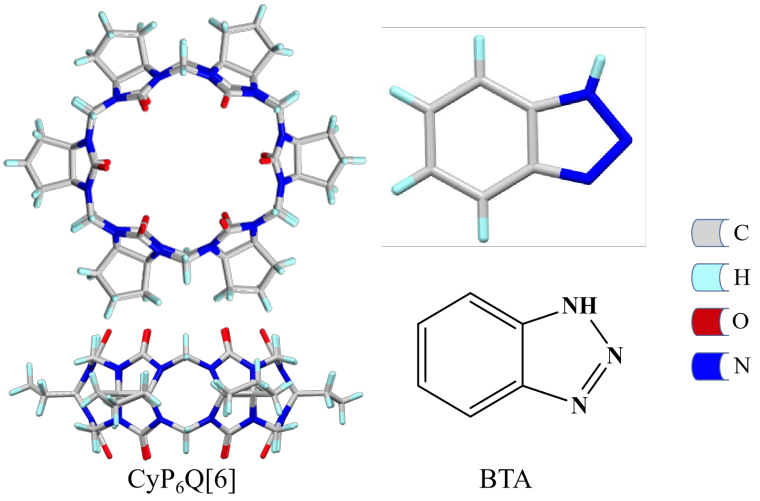

Figure 1. Structures of $CyP_6Q[6]$ and the guest molecules used in this study.

Experimental

Experimental equipment and reagents

Data were collected on the following instruments: JNM-ECZ 400sMHz NMR spectrometer, G6500 mass spectrometer (Agilent), ITC, VERTEX70 Fourier IR spectroscopy, BXT-TBDY-1250 thermogravimetric analysis, and a Bruker D8 VENTURE single crystal diffractometer.

The compound $CyP_6Q[6]$ prepared by our research group. All other reagents were purchased commercially and were analytically pure.

Determination by ^{1}H NMR spectroscopy

The compound $CyP_6Q[6]$ was prepared in D_2O as a solution of 1.0×10^{-3}mol/L and was added dropwise to a D_2O solution of 2.0×10^{-3} mmol/L guest (BTA) before determining on a Varian INOVA-400 M NMR spectrometer at 20℃.

Determination by ITC

Isothermal titration calorimetry was measured on a NanoITC (TA, USA). The measurements and data processing methods are as reported in the literarure [34].

Determination by mass spectrometry

Mass spectrometry was performed as reported previously [34].

Determination by mass IR

IR testing of BTA and $CyP_6Q[6]$ references[35].

Determination by mass thermogravimetric

Thermogravimetric tests of BTA and CyP6Q[6][35].

Synthesis of complex

Accurately weigh 0.006g $CyP_6Q[6]$ (0.005mmol) and 0.001g BTA(0.01mmol) into a clean 5mL bottle of vials, add 3ml of hydrochloric acid solution with a concentration of 3mol/L and heat the mixture until it is completely dissolved, so that the solvent can evaporate and crystallize naturally. The colorless transparent BTA@$CyP_6Q[6]$ crystal was obtained with a yield of 15.3%.

Crystallography

Determination of crystal structure References [33]. The main crystal structure parameters are shown in Table 1 (archived as CCDC:2267077).

Table. 1 The main crystallographic data of the complex

BTA@$CyP_6Q[6]$	
Formula	$C_{60}H_{65}Cl_8N_{27}O_{12}Zn_2$
M_r	1770.73
Crystal	monoclinic
Space group	*C*2/c
a (Å)	27.119(6)
b (Å)	17.959(4)
c (Å)	18.348(5)

α (deg)	90
β (deg)	94.413(6)
γ (deg)	90
Z	4
Dc (g cm $^{-3}$)	1.320
μ (mm $^{-1}$)	0.844
R_{int}	0.1831
GOF (F^2)	1.101
R_1[I > 2σ(I)][a]	0.1102
wR[I > 2σ(I)][b]	0.3007
R (all data)	0.1775
wR_2 (all data)	0.3339

Results and discussion

^{1}H NMR spectroscopic analysis

The host-guest interaction mode between BTA and CyP$_6$Q[6] was investigated by ^{1}H NMR spectroscopy. The results show that after CyP$_6$Q is added into D_2O solution of BTA, the α and β chemical signal peaks of BTA are shifted to the high field, and the moving distance is 0.36~0.66 ppm. It shows that guest molecules enter the cavity of CyP$_6$Q[6]. Due to the shielding action of the cavity of CyP$_6$Q[6], the symmetric CyP$_6$Q[6] becomes asymmetric, thus splitting the nuclear magnetic signal (as shown in Fig. 2). There is obvious host-guest interaction between BTA and CyP$_6$Q[6].

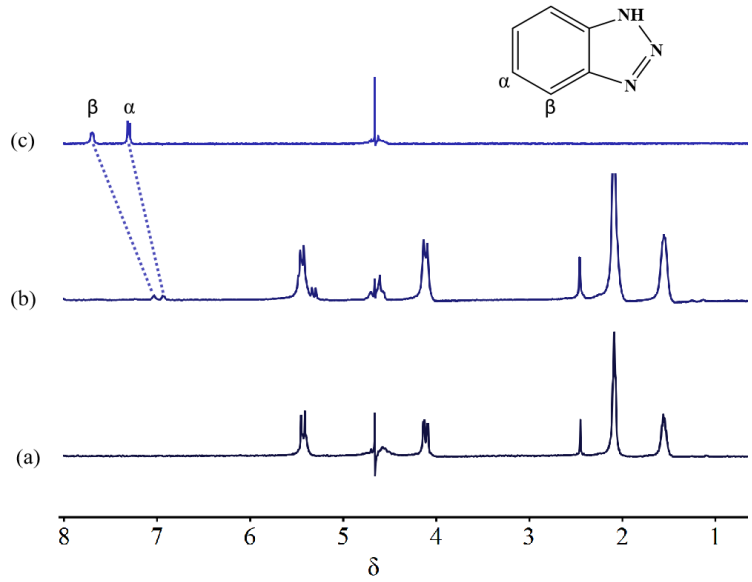

Figure 2. ^{1}H NMR titration spectra (400 MHz, D_2O, 25°C): **(a)** ^{1}H NMR spectrum of CyP$_6$Q[6] (0.5mM); **(b)** ^{1}H NMR spectrum of BTA@CyP$_6$Q[6]; **(c)** free guest BTA.

ITC Analysis

ITC (see Fig. 1 for support materials) and Table. 2 show the isothermal curves and thermodynamic parameters of the interaction between $CyP_6Q[6]$ and BTA. It can be seen from the data that the reaction is mainly driven by enthalpy and the binding constant is 4.09×10-5mol L^{-1}.

Table 2. ITC measurements of the thermodynamics parameters of BTA and $CyP_6Q[6]$ interactions at 298.15 K

Experiment	BTA@$CyP_6Q[6]$
Model	Independent
Ka/(L mol^{-1})	4.09×10^{-5}
ΔH/(KJ mol^{-1})	-21.70
TΔS/(KJ mol-1)	-10.33

HPLC-QTOF Mass Spectrometry Analysis

The interaction mode of host and guest in BTA@$CyP_6Q[6]$ was investigated by MALDI-TOF mass spectrometry. The molecular ion peak presented an obvious signal peak at m/z = 1357.02539 (the theoretical value of m/z is1356.357) (see supporting material Fig. 2). BTA and $CyP_6Q[6]$ form a host-guest inclusion complex, namely $[CyP_6Q[6]+BTA+H]^+$. This result showed that there is an interaction mode of 1∶1 between the host and guest, which is consistent with the results of single crystal data.

IR spectral analysis

Figure. 3 shows the IR spectra recorded for (a) $CyP_6Q[6]$, (b) BTA , (c) a physical mixture of $CyP_6Q[6]$ and BTA {n($CyP_6Q[6]$)/n(BTA) = 1:1} and (d) the BTA@$CyP_6Q[6]$ inclusion complex . The object BTA has δ-C-H out-of-plane bending vibration peaks at 705 ~ 775 cm^{-1}, υ-C-N stretching vibration peak was observed at 1012 cm^{-1} and υ-N=N stretching vibration peak was observed at 1207 cm^{-1} (as shown in Fig. 3b). As shown in Fig. 3c, the spectral line (c) is a simple superposition of the infrared spectral lines of BTA and $CyP_6Q[6]$ (a) and TBA (b), and there is no interaction. The characteristic peaks at 1012 cm^{-1} and 1207 cm^{-1} disappeared obviously, while the peaks at 705~775 cm^{-1} weakened significantly. It can be concluded that BTA enters the cavity of $CyP_6Q[6]$ through hydrogen bonding and dipole interaction, forming BTA@$CyP_6Q[6]$ inclusion complex.

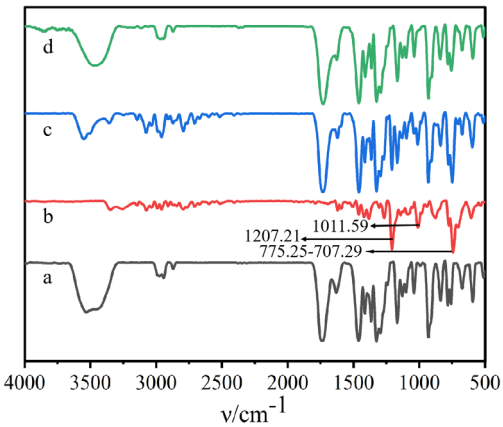

Figure 3. **(a)** IR spectra recorded for $CyP_6Q[6]$; **(b)** IR spectra recorded for BTA; **(c)** a physical mixture of $CyP_6Q[6]$ and BTA ; **(d)** and the BTA@$CyP_6Q[6]$ inclusion complex.

Thermogravimetric Analysis

TGA and DTG of G1, G1@$CyP_6Q[6]$, and $CyP_6Q[6]$ are shown in Fig. 5. As can be seen from Fig. 5, $CyP_6Q[6]$ had good thermal stability due to its rigid structure. The mass decline area before 139℃ was the dehydration process, and the mass reduced by 10.47%. There was no obvious decomposition phenomenon in the temperature range of 139℃~355℃. The decomposition began at 400℃, and the weight loss rate reached 84.43% at 542℃. Due to the low thermal stability of BTA itself, it began to decompose at about 186℃ and completely decomposed at 280℃. TBA@CyP6Q[6] decomposed at 347℃ and completely decomposed at 510℃. The results showed that the TBA@$CyP_6Q[6]$ inclusion complex had a higher decomposition temperature, less mass variation and better thermal stability than TBA alone.

The TBA has a melting heat absorption peak at 266℃, while $CyP_6Q[6]$ has two heat absorption peaks at 403.8℃ and 505.8℃. For the TBA@$CyP_6Q[6]$ inclusion complex, the melting absorption peak of TBA at 266℃ and the endothermic peaks of $CyP_6Q[6]$ at 403.8℃ and 505.8℃ disappeared, while new heat absorption peaks appeared at 388℃ and 486℃. The results showed that TBA formed an inclusion complex with the $CyP_6Q[6]$, and the addition of $CyP_6Q[6]$ had a obvious release effect in the decomposition rate of TBA. The stability of the complex is between that of BTA and $CyP_6Q[6]$. It was further proved that BTA entered the cavity of the $CyP_6Q[6]$ and enhanced the thermal stability of TBA.

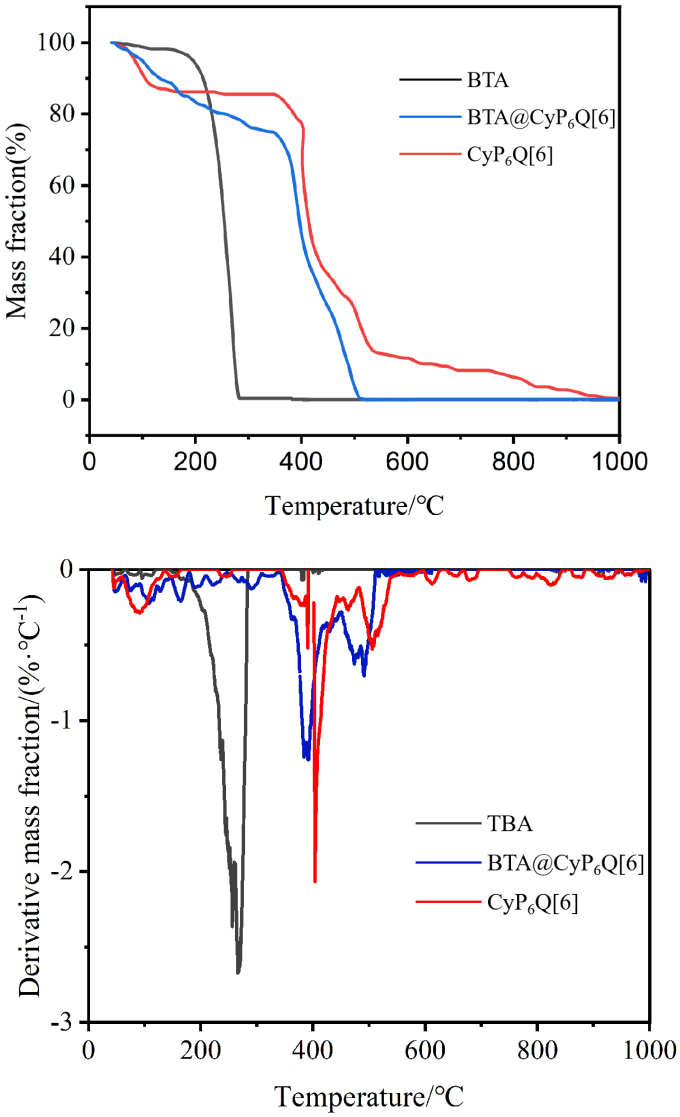

Figure 5. TGA and DTG curves of BTA, BTA@$CyP_6Q[6]$ and $CyP_6Q[6]$.

Description of Crystal Structures

The cucurbit[*n*]urils have a cavity with neutral electrostatic potential, a carbonyl port with negative electrostatic potential and an outer wall with positive electrostatic potential. This structural feature promotes the interaction between guest molecules and cucurbit[*n*]urils to form a cucurbit[*n*]uril-based supramolecular framework. $CyP_6Q[6]$ and BTA mainly through hydrogen bonding and dipole interaction, the structure shown in Figure. 6a. It can be seen from Fig. 6b that there is a dipole-dipole interaction between the nitrogen atom (N14) of BTA and the portal carbonyl oxygen atom (O1, O4, O5) of $CyP_6Q[6]$. Another nitrogen atom (N15) linked to hydrogen is connected to the oxygen atoms (O2, O3) at cucurbit[*n*]urils port through hydrogen bonds. Where N14···O1, N14···O4, N14···O5, N15-H15···O2 and N15-H15···O3, the interaction distances of they are 3.041, 2.729, 2.735, 2.553 and 1.920Å. In addition, hydrogen bonding (C-H···N) exists between the carbon atoms (C28, C31) on the benzene ring of BTA and the

nitrogen atoms (N9, N10) in the cavity of $CyP_6Q[6]$ (as shown in Figure. 3c). The interaction distances between C28-H28···N9 and C31-H31···N10 are 2.599 and 2.608 Å, respectively. The results show that BTA entered the cavity of $CyP_6Q[6]$, and a supermolecule assembly of 1:1 BTA@$CyP_6Q[6]$ is formed by abundant hydrogen bonds and dipole interactions.

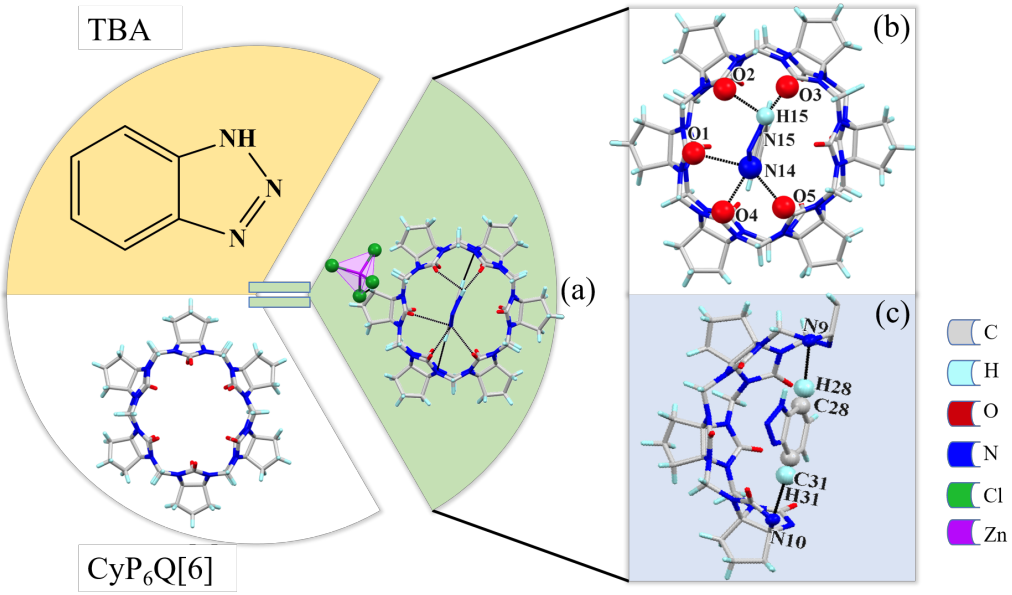

Figure 6. Crystal diagram of the complex: **(a)** supramolecular self-assembly of the complex; **(b,c)** interaction between BTA@$CyP_6Q[6]$.

As shown in Figure. 7, each $CyP_6Q[6]$ is surrounded by eight $[ZnCl_4]^{2-}$. $[ZnCl_4]^{2-}$ is linked to methylene hydrogen on the outer surface of $CyP_6Q[6]$ molecule by C-H···Cl ion-dipole interaction. The interaction distances of C8-H8B···Cl3, C14-H14B···Cl1, C21-H21A···Cl3 and C23-H23B···Cl4 are 2.630, 2.942, 2.638 and 2.912 Å (Figure. 7a-c).

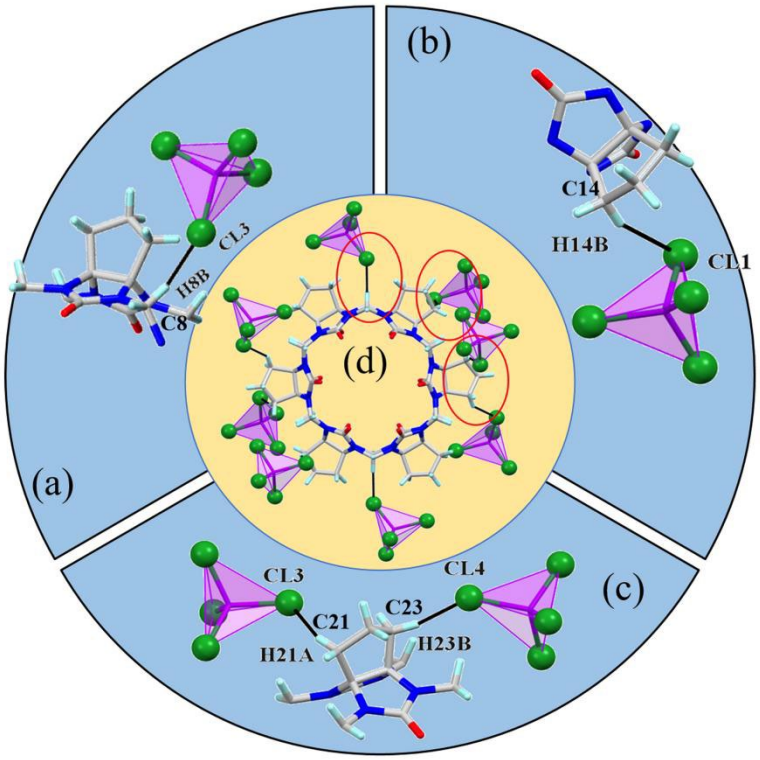

Figure 7. X-ray crystal structures of $[ZnCl_4]^{2-}$-induced $CyP_6Q[6]$-based porous supramolecular assembly; **(a,b,c)** features of the interaction between the $CyP_6Q[6]$ molecule and $[ZnCl_4]^{2-}$ anions.

Figure 8a shows a two-dimensional stacked structure of the complex in the c-axis direction. It can be seen that $[ZnCl_4]^{2-}$ with BTA @ $CyP_6Q[6]$ constituted an ' 8 ' -shaped honeycomb porous supramolecular structure. Further analysis showed that $ZnCl_4]^{2-}$and $CyP_6Q[6]$ constructed a one-dimensional supramolecular long chain of ABAB type (AB is the orientation of two $CyP_6Q[6]$) through C-H... O hydrogen bonding and C-H... Cl ion-dipole interaction. (As shown in Figure. 8b and 8c). In addition, there are a large number of elliptical holes in the plane accumulation diagram. The length of the long and short half-axes is 4.64Å and 2.87Å, respectively. The angle between the two orientations of the cucurbit[*n*]urils is 69.33°，and the hole area is approximately 41.81 $Å^2$. which is slightly larger than the port area of $CyP_6Q[6]$, and can be used to separate substances with molecular diameter between the two. This structure has potential application value in the fields of molecular adsorption and drug carrier.

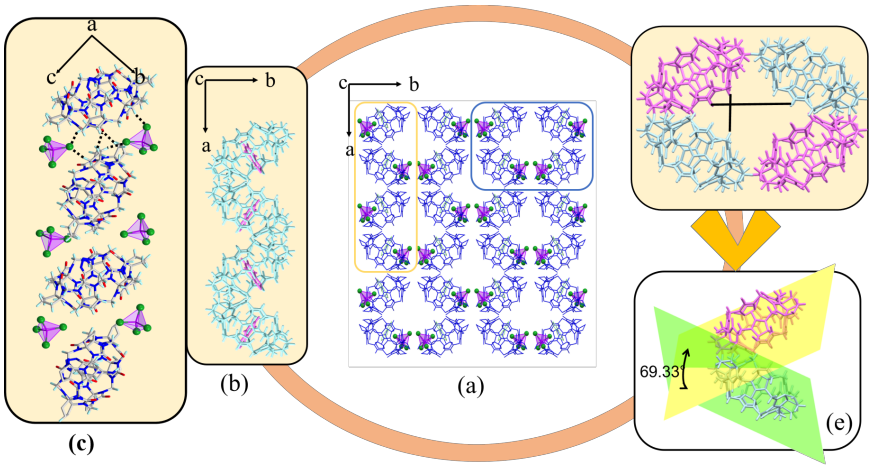

Figure 8. **(a)** BTA@CyP$_6$Q[6] stacked graph along the c-axis. **(b,c)** a zigzag CyP$_6$Q[6] molecule chain; **(d ,e)** overall view of the CyP$_6$Q[6]-based porous supramolecular assembly.

Conclusions

Taking BTA as a guest molecule, the interaction mode between BTA and CyP$_6$Q[6] has been investigated by using single crystal X-ray diffraction, ^{1}H NMR spectroscopy, isothermal titration calorimetry (ITC), MALDI-TOF mass spectrometry, IR spectroscopy and thermogravimetric analysis. The results show that the benzene part of BTA enters the cavity of CyP6Q[6], and the triazole part is located in the port of CyP$_6$Q[6], with an action ratio of 1:1. Eight $[ZnCl_4]^{2-}$ are enriched around one CyP$_6$Q[6]. The CyP$_6$Q[6] mainly combines with TBA through enthalpy drive to enhance the thermal stability of TBA. The three components (BTA, Cy$_{P6}$Q[6], $[ZnCl_4]^{2-}$) construct a supramolecular assembly with dense pores in the *c* direction through hydrogen bonding, dipole-dipole and ion-dipole interaction. It has potential application value in the fields of molecular adsorption, separation and drug carrier.

References

[1] Vicens, J., & Vicens, Q. (2011). Emergences of supramolecular chemistry: from supramolecular chemistry to supramolecular science. ***J. Incl. Phenom. Macrocycl.***, 71(3-4): 251-274. http://10.1007/s10847-011-0001-z

[2] Kolesnichenko, I. V., & Anslyn, E. V. (2017). Practical applications of supramolecular chemistry. ***Chem. Soc. Rev.***, 46(9): 2385-2390. http://10.1039/c7cs00078b

[3] van Dun, S., Ottmann, C., Milroy, L. G., & Brunsveld, L. (2017). Supramolecular Chemistry Targeting Proteins. ***J. Am. Chem. Soc.***, 139(40): 13960-13968. http://10.1021/jacs.7b01979

[4] Zhou, C., Gan, L., Zhang, Y., Zhang, F., Wang, G., Jin, L., & Geng, R. (2009). Review on supermolecules as chemical drugs. ***Sci. China Ser. B: Chem.***, 52(4): 415-458. http://10.1007/s11426-009-0103-2

[5] Barba B, A., Nilam, M., & Hennig, A. (2020). Supramolecular Chemistry in the Biomembrane. ***ChemBioChem.***, 21(7): 886-910. http://10.1002/cbic.201900646

[6] Lee, J. W., Samal, S., Selvapalam, N., Kim, H. J., & Kim, K. (2003). Cucurbituril homologues and derivatives: new opportunities in supramolecular chemistry. ***Acc. Chem. Res.***, 36(8): 621-630. http://10.1021/ar020254k

[7] Chen, K., Cong, H., Xiao, X., Zhang, Y.-Q., Xue, S.-F., Tao, Z., Zhu, Q.-J., & Wei, G. (2011). Hydroquinone-induced framework based on direct coordination of rubidium ions to cucurbit[7]uril. ***CrystEngComm***, 13(16). http://10.1039/c1ce05048f

[8] Chen, K., Liang, L. L., Liu, H.-J., Tao, Z., Xue, S.-F., Zhang, Y. Q., & Zhu, Q. J. (2012). *p*-Hydroxybenzoic acid-assisted homochiral 1D-helical coordination polymers from calcium cations and cucurbit[5]uril. ***CrystEngComm***, 14(23). http://10.1039/c2ce25958c

[9] Combes, S., Tran, K. T., Ayhan, M. M., Karoui, H., Rockenbauer, A., Tonetto, A., Monnier, V., Charles, L., Rosas, R., Viel, S., Siri, D., Tordo, P., Clair, S., Wang, R., Bardelang, D., & Ouari, O. (2019). Triangular Regulation of Cucurbit[8]uril 1:1 Complexes. ***J. Am. Chem. Soc.***, 141(14): 5897-5907. http://10.1021/jacs.9b00150

[10] Chen, K., Hua, Z. Y., Zhao, J. L., Redshaw, C., & Tao, Z. (2022). Construction of cucurbit[*n*]uril-based supramolecular frameworks via host–guest inclusion and functional properties thereof. ***Inorg. Chem. Front.***, 9(12): 2753-2809. http://10.1039/d2qi00513a

[11] Pan, S., Saha, R., Mandal, S., Mondal, S., Gupta, A., Fernández Herrera, M. A., Merino, G., & Chattaraj, P. K. (2016). Selectivity in Gas Adsorption by Molecular Cucurbit[6]uril. ***J. Phys. Chem. C***, 120(26): 13911-13921. http://10.1021/acs.jpcc.6b02545

[12] Jiao, Y., Xu, J. F., Wang, Z., & Zhang, X. (2017). Visible-Light Photoinduced Electron Transfer Promoted by Cucurbit[8]uril-Enhanced Charge Transfer Interaction: Toward Improved Activity of Photocatalysis. ***ACS Appl. Mater. Interfaces***, 9(27): 22635-22640. http://10.1021/acsami.7b07026

[13] Luo, Y., Zhang, W., Yang, X. N., Yang, M. X., Min, W., Tao, Z., & Xiao, X. (2022). Cucurbit[10]uril-Based Orthogonal Supramolecular Polymers with Host-Guest and Coordination Interactions and Its Applications in Anion Classification. ***Inorg. Chem.***, 61(42): 16678-16684. http://10.1021/acs.inorgchem.2c02333

[14] Hirani, Z., Taylor, H. F., Babcock, E. F., Bockus, A. T., Varnado, C. D., Jr., Bielawski, C. W., & Urbach, A. R. (2018). Molecular Recognition of Methionine-Terminated Peptides by Cucurbit[8]uril. ***J. Am. Chem. Soc.***, 140(38): 12263-12269. http://10.1021/jacs.8b07865

[15] Liu, M., Cen, R., Li, J., Li, Q., Tao, Z., Xiao, X., & Isaacs, L. (2022). Double-Cavity Nor-Seco -Cucurbit[10]uril Enables Efficient and Rapid Separation of Pyridine from Mixtures of Toluene, Benzene, and Pyridine. ***Angew. Chem. Int. Ed. Engl.***, 61(35): e202207209. http://10.1002/anie. 202207209

[16] Xiao, H., Yang, X., Yang, L., Yang, D., Luo, Y., Yang, H. P., Tao, Z., Xiao, X., & Li, Q. (2022). Cucurbit [8] uril-based supramolecular fluorescent biomaterials for cytotoxicity and imaging studies of kidney cells. ***Front. Chem.***, 10: 974607. http://10.3389/fchem.2022.974607

[17] Yang, D., Luo, Y., Yuan, S. W., Chen, L. X., Ma, P. H., Tao, Z., & Xiao, X. (2023). A cucurbit[8]uril-based supramolecular polymer constructed via outer surface interactions: Use as a sensor, in cellular imaging and beyond. ***J. Mol. Liq.***, 379. http://10.1016/j.molliq.2023.121593

[18] Samanta, S. K., Quigley, J., Vinciguerra, B., Briken, V., & Isaacs, L. (2017). Cucurbit[7]uril Enables Multi-Stimuli-Responsive Release from the Self-Assembled Hydrophobic Phase of a Metal Organic Polyhedron. ***J. Am. Chem. Soc.***, 139(26): 9066-9074. http://10.1021/jacs.7b05154

[19] Zhao, H., Shen, F. F., & Sun, J. F. (2022). Cucurbit[8]uril-controlled [2 + 2] photodimerization of styrylpyridinium molecule. ***Inorg. Chem. Commun.***: 141

[20] Lim, S., Kim, H., Selvapalam, N., Kim, K. J., Cho, S. J., Seo, G., & Kim, K. (2008). Cucurbit[6]uril: Organic Molecular Porous Material with Permanent Porosity, Exceptional Stability, and Acetylene Sorption Properties. ***Angew. Chemie***, 120(18): 3400-3403. http://10.1002/ange.200800772

[21] Lin, R. L., Liu, J. X., Chen, K., & Redshaw, C. (2020). Supramolecular chemistry of substituted cucurbit[*n*]urils. ***Inorg. Chem. Front.***, 7(17): 3217-3246. http://10.1039/d0qi00529k

[22] Day, A., Arnold, A., & Blanch, R. (2003). A Method for Synthesizing Partially Substituted Cucurbit[*n*]uril. ***Molecules***, 8(1): 74-84. http://10.3390/80100074

[23] Ayhan, M. M., Karoui, H., Hardy, M., Rockenbauer, A., Charles, L., Rosas, R., Udachin, K., Tordo, P., Bardelang, D., & Ouari, O. (2015). Comprehensive Synthesis of Monohydroxy-Cucurbit[n]urils (n = 5, 6, 7, 8): High Purity and High Conversions. ***J. Am. Chem. Soc.***, 137(32): 10238-10245. http://10.1021/jacs.5b04553

[24] Isobe, H., Sato, S., & Nakamura, E. (2002). Synthesis of disubstituted cucurbit[6]uril and its rotaxane derivative. ***Org. Lett.***, 4(8): 1287-1289. http://10.1021/ol025749o

[25] Zhao, Y., Mandadapu, V., Iranmanesh, H., Beves, J. E., & Day, A. I. (2017). The Inheritance Angle: A Determinant for the Number of Members in the Substituted Cucurbit[n]uril Family. ***Org. Lett.***, 19(15): 4034-4037. http://10.1021/acs.orglett.7b01786

[26] Zhao, J., Kim, H.-J., Oh, J., Kim, S. Y., Lee, J. W., Sakamoto, S., Yamaguchi, K., & Kim, K. (2001). Cucurbit[*n*]uril Derivatives Soluble in Water and Organic Solvents. ***Angew. Chemie Int. Ed.***, 40(22): 4233-4235. http://10.1002/1521-3773(20011119)40:22

[27] Wu, F., Wu, L. H., Xiao, X., Zhang, Y. Q., Xue, S. F., Tao, Z., & Day, A. I. (2012). Locating the cyclopentano cousins of the cucurbit[*n*]uril family. ***J. Org. Chem.***, 77(1): 606-611. http://10.1021/jo2021778

[28] Mutihac, R. C., Bunaciu, A. A., Buschmann, H. J., & Mutihac, L. (2020). A brief overview on supramolecular analytical chemistry of cucurbit[*n*]urils and hemicucurbit[*n*]urils. ***J. Incl. Phenomen. Macrocycl.***, 98(3-4): 137-148. http://10.1007/s10847 -020-01019-5

[29] Liu, S., Kim, K., & Isaacs, L. (2007). Mechanism of the conversion of inverted CB[6] to CB[6]. ***J. Org. Chem.***, 72(18): 6840-6847.http://10.1021/jo071034t

[30] Jin, Y. M., Meng, Y., Yang, X. N., Zhu, C., Tao, Z., Liu, J. X., & Ma, P. H. (2021b). Supramolecular Frameworks Constructed by Exclusion Complexes of Symmetric Dicyclohexanocucurbit[6]uril with Benzene Ring-Containing Guests. ***Crystal Growth & Design***, 21(5): 2977-2985. http://10.1021/acs.cgd.1c00138

[31] Jin, Y., Huang, T., Zhao, W., Yang, X., Meng, Y., & Ma, P. (2020). A study on the self-assembly mode and supramolecular framework of complexes of cucurbit[6]urils and 1-(4-methoxyphenyl)piperazine. ***RSC Adv.***, 10(61): 37369-37373. http://10.1039/d0ra07988j

[32] Zheng, J., Jin, Y. M., Yang, X. N., Zhang, L., Jiang, D. F., Zhao, W. W., Meng, Y., Gao, J., & Ma, P. H. (2021a). Self-Assembly Mode and Supramolecular Framework of

Cyclopentanocucurbit[6]uril and Aromatic Amines. ***Curr. Org. Chem.*** (23): 25

[33] Zheng, J., Zhao, W. W., Meng, Y., Jin, Y. M., Gao, J., & Ma, P. H. (2021b). Supramolecular Self-Assembly of Cyclopentyl-Substituted Cucurbit[n]uril with Fe^{3+}, Fe^{2+}, and $HClO_4$ Based on Outer Surface Interaction. ***Cryst. Res. Technol.***, 56(3). http://10.1002/crat. 202000183

[34] Jin, Y. M., Jiang, D. F., Meng, Y., Gao, J., Zheng, J., & Ma, P.-H. (2021a). Crystal structure of self-assembled inclusion complex of symmetric dicyclohexanocucurbit[6]uril with 1H-benzotriazole. ***J. Incl. Phenom. Macrocycl.***, 100(3-4): 209-215.http://10.1007/s10847-021-01076-4

[35] Yang, N., Dai, X., Ma, Y., Yang, X., & Ma, P. (2023b). Study on the Host-Guest Interactions Between Tetramethyl Cucurbit[6]uril and Benzimidazole Derivatives. ***Chem. Res. Chin. Uni.***. http://10.1007/s40242-023-3078-1